Formation Mechanism, Growth Kinetics and Stability Limits of Graphene Adlayers in Metal Catalyzed CVD Growth

Zhu-Jun Wang[1], Feng Ding[2,3], Gyula Eres[4], M. Antonietti[5], R. Schloegl[1], Marc Georg Willinger[1,5*]

[1] Department of Inorganic Chemistry, Fritz Haber Institute of the Max Planck Society, Berlin-Dahlem D-14195, Germany. [2] Center for Multidimensional Carbon Materials (CMCM), Institute for Basic Science (IBS), Ulsan 44919, Republic of Korea. [3] School of Materials Science and Engineering, Ulsan National Institute of Science and Technology, Ulsan 44919, Republic of Korea. [4] Materials Science and Technology Division, Oak Ridge National Laboratory, Oak Ridge, Tennessee 37831, USA. [5] Department of Colloid Chemistry, Max Planck Institute of Colloids and Interfaces, Potsdam, D-14424, Germany

Correspondence and requests for materials should be addressed to M.G.W. (email: marc.willinger@scopem.ethz.ch).

[*]Now at: Scientific Center for Optical and Electron Microscopy, ScopeM, ETH Zürich, 8093 Zürich, Switzerland

Abstract

We discuss a new mechanism by which catalytic chemical vapor deposition of graphene spontaneously terminates at a single-layer on Pt foils. This self-limited growth regime was identified by direct imaging of adlayer graphene evolution using *in situ* environmental scanning electron microscopy. Our data reveal that adlayer formation occurs by two fundamentally different nucleation events. Primary nucleation is the standard nucleation that occurs only at the onset of growth. We report the first observation of secondary nucleation of adlayer graphene that occurs near full coverage, by merging and coalescence of single layer domains. From the onset of growth, the bottom layer coupled to Pt always grows faster than the adlayers. The most important result revealed by this work is that the dynamic equilibrium between the forward reaction of carbon incorporation and the reverse reaction of graphene etching is layer specific and gives rise to a spontaneous reversal of adlayer evolution from growth to etching. The growth reversal has important practical benefits. It creates a self-limited growth regime in which all adlayer graphene is removed and enables large scale production of 100 % single layer graphene.

Introduction

Nucleation processes at surfaces play a crucial role in the growth of crystals and thin films. Knowledge about the relation between growth kinetics and nucleation behavior is specifically important in the case of two-dimensional materials such as graphene, where in-plane nucleation influences the quality of the film and the addition of each

individual layer induces discrete changes in the electronic structure. The development of growth methods capable of achieving complete layer termination with atomically sharp interfaces has been a longstanding challenge in practical thin film growth. A growth mode that can potentially achieve complete coverage in epitaxial thin film growth is known as layer-by-layer (LBL) or Frank-van der Merwe growth. In actual film growth, a breakdown of LBL growth results in nucleation of islands on top of the growing layer before it reaches full coverage.

Graphene is a prototype 2D material, and graphene growth represents a model system for understanding 2D growth processes. The most widely applied method for the production of single-layer graphene (SLG) and vertically stacked few-layer graphene (FLG) is based on metal catalyzed chemical vapor deposition (CVD) growth.[1-6] Among the various catalysts that are used for this process, Pt offers a quite large parameter space for SLG/FLG growth, stemming from its high catalytic activity for hydrocarbon dissociation.[7] Indeed, undesired formation of carbon layers on platinum nanoparticles and carbon coking is a long standing problem in the field of hydrocarbon catalysis.[8] Owned to the high catalytic activity, the growth of purely single layer graphene on Pt has been extremely challenging. Formation of FLG has been reported even when using highly diluted hydrocarbon feeds with hydrocarbon to hydrogen ratios of 4:700.[2]

Industrial scale production of single layer graphene requires a robust control over the formation of adlayers and thus, mechanistic insight on the underlying kinetic processes. In this respect, methods that enable direct spatially- and time-resolved observation of graphene growth have dramatically accelerated our understanding of 2D growth.[4,9-22]

We recently demonstrated the power of *in situ* SEM imaging for the study of graphene growth under controlled atmosphere and relevant catalytic CVD conditions.[23-26] It enables real-time observation of the complete CVD growth process including substrate annealing, film nucleation and growth and finally, growth termination and substrate cooling at variable magnification and nm scale lateral resolution.

Using this instrument, we are able to reveal, for the first time, two fundamentally different mechanisms of adlayer formation, their respective growth regimes and stability limits. We show that adlayers either nucleate simultaneously with SLG on surface steps or defects during primary nucleation at the onset of growth, or form by secondary nucleation during the merging and coalescence between already growing single layer domains. Direct observation of layer dependent growth kinetics under different growth conditions reveals how the evolution of adlayers is controlled by diffusion processes and related to the interaction between the first layer and the substrate. We show that the competition between the forward reaction step of growth and the reverse reaction step of graphene etching eventually results in complete removal of all adlayers, all the while the base layer in contact with Pt continuous growing. The growth reversal and etching of adlayers is of practical significance. It enables the

complete removal of adlayer graphene and ensures that graphene growth is terminated at a single layer across the entire growth surface.

Results and discussion

Prior to CVD growth, polycrystalline Pt foils were annealed under 25 Pa H_2 atmosphere at 900 °C for up to 24 hours in order to remove surface contaminations and to increase the size of the platinum grains (see Supplementary Movie M1). The long annealing time is required in order to remove bulk dissolved carbon to a degree at which no more precipitation of carbon from the bulk can be observed during cooling. After annealing, CVD graphene growth was induced by adding C_2H_4 to the H_2 flow.[23]

Graphene growth

Formation of graphene can generally be observed after an induction period during which the surface of the metal catalyst supersaturates in growth species.[24,27] For a given temperature, the nucleation density is strongly depending on the C_2H_4/H_2 ratio (See Supplementary Figure 1).[28] During growth, each graphene domain expands through the attachment of carbon species at the growth front.[9] For growth at 900 °C on polycrystalline Pt, we observed a grain dependent growth behavior. It is characterized by a variation in the induction period, nucleation density and growth speed, and is a consequence of the grain orientation dependent surface structure and associated catalytic properties of Pt.[28] Furthermore, a characteristic grain orientation dependent growth of similarly shaped and aligned domains can be observed (See Supplementary Figure 2). The anisotropic growth behavior is induced by graphene edge attachment at Pt steps and a different growth speed along and across terraces and thus, a consequence of the Pt surface structure (See Supplementary Figure 3).[23] Similar anisotropic growth behavior was observed in graphene grown on ruthenium[4] and associated with orientation dependent diffusion processes.[29] Because of the high catalytic activity, there is a large parameter space in which graphene growth on Pt proceeds in the attachment limited regime.[30] In this regime, the net number of carbon atoms that are attached to an island per unit time is proportional to its perimeter, and the radial growth rate is constant along the different growth directions (see Supplementary Figure 3). A clear sign of attachment-limited growth is that the growing islands maintain their specific polygonal shape with smooth edges and sharp vertexes throughout the growth.[24,31]

Adlayer formation:

Besides single layer graphene, the formation of few-layer graphene is frequently observed during CVD growth. In order to study the mechanisms of adlayer formation, we performed experiments under two different growth conditions.

Under quasi-equilibrium conditions, graphene growth is very slow. In this case, the hydrocarbon flux is set to the minimal value required to achieve surface supersaturation, nucleation and growth of graphene. Under these conditions, the rate of growth species production by catalytic decomposition on the Pt substrate just slightly exceeds the rate of their loss from the surface due to desorption and gasification. In our set-up, quasi-equilibrium growth was achieved by a slow and step-wise increase of the C_2H_4 flow until graphene growth could be observed at a C_2H_4/H_2 flow ratio of ~ 0.1:10 sccm and a total pressure of 25 Pa. The resulting radial growth speed of graphene domains, measured by real-time imaging, was below 10 nm/s.

A roughly tenfold increase of the C_2H_4:H_2 ratio to 1.2:10 sccm at a total pressure of 25 Pa at 900 °C generates a more than 50-fold increase in the growth rates of > 500 nm/s, and a different growth regime that we refer to as non-equilibrium growth.

1. Primary adlayer nucleation

The slow growth rate of graphene under quasi equilibrium conditions enables unobscured observation of isolated islands, and is ideally suited for real-time imaging of adlayer formation and evolution.

FLG islands appear at the onset of growth, simultaneously with the dominant appearance of SLG domains. They can be distinguished from SLG on the based on their strong contrast. When they first appear in the SEM image as small dark dots after nucleation, the outline of the individual layers in the vertical FLG stack cannot be resolved. With time of growth, however, the individual layers become visible. An apparent difference in their respective growth rates gives rise to a lateral separation of the growth fronts and thus, to identifiable steps in SEM image contrast for each individual layer (see Figure 1 a-d). The growth behavior of the different layers can be analyzed based on the recorded images as shown in Figure 1a-d. The image stack recorded during growth is represented by one frame in (a) and orthogonal views through the image stack in (b) and (c). The orthogonal views correspond to cuts through planes containing the time axis. In (d), a three-dimensional view of the image stack is shown (see Supplementary Movies M3 and M4). The orthogonal views reveal the evolution of the contrast due to the first, second and third layer and indicate that all layers nucleated simultaneously. Interestingly, the individual layers of such a stack grow self-similar in the shape of truncated hexagons, indicating that each adlayer is co-oriented and similarly attached to a Pt surface step (see Supplementary Figure 3). Thus, substrate structure and associated

barriers along and across steps, as well as growth modulation due to attachment to a Pt step have a similar influence on the growth behavior of individual layers in a FLG stack. The slopes at which the areas of constant contrast increase with time in the orthogonal views in Figure 1 b and c represent the growth rates of the different layers along the directions defined by the cutting planes. It is evident that the growth rates are higher in the case of the first layer. The evolution of the integral area and perimeter of the first and second layer are shown in (e). While the faster growing first layer shows an attachment limited, nearly constant radial growth and associated square-function like increase in area, the second layer shows a sigmoidal growth behavior.

Adlayer nucleation at surface steps is the only mechanism observed under quasi-equilibrium growth conditions and schematically shown in Figure 3a.

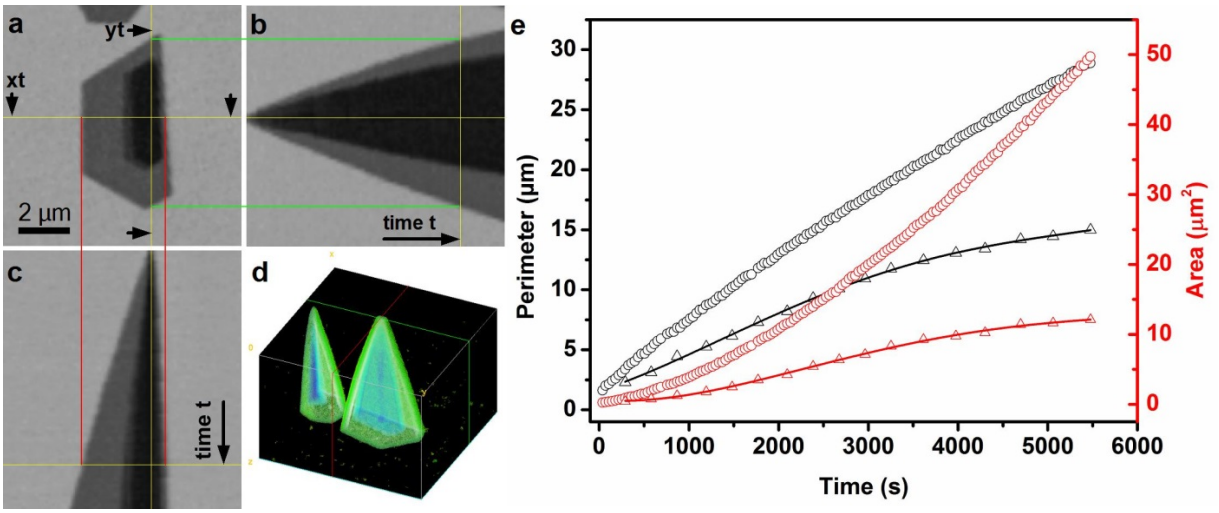

Figure 1. The early stages of adlayer growth: (a-d) Orthogonal views through an image stack recorded during the growth of a FLG at a Pt step edge (not visible). The yellow lines in (a), (b), and (c) indicate the cutting planes and position in the 3D stack, respectively. The time axis runs from 0 sec to 2h. (d) shows a three-dimensional representation of the temporal evolution. (e) shows the evolution of the perimeter and area of the first (circle) and second (triangle) layer with time (see Supplementary Movie 3 and 4).

2. Secondary adlayer nucleation

In the case of non-equilibrium growth conditions, however, two additional mechanism of adlayer formation could be identified. They are both related to processes that occur during the merging and coalescence of adjacent SLG domains at a later stage of growth. They are thus referred to as secondary adlayer nucleation. In the case of co-oriented single layer domains growing on the same Pt grain, the merging of parallel growth fronts can give rise to the initiation of a single adlayer. The fact that only one adlayer is formed, combined with the observation that the

newly formed layer grows concentrically in all directions, leads us to the conclusion that it nucleates from a defect at the grain boundary between the two coalescing SLG domains. This is the second mechanism and exemplified in Figure 3b. Alternatively, the adlayer could be formed through a continued growth of either of the two or both SLG sheets if one of them locally overgrows the other one. Depending on the details of the merging process, one or more screw dislocations would then be induced, giving rise to the initiation of a single or double spiral and thus, the formation of multiple adlayers. This is the third mechanism of adlayer formation and exemplified by *in situ* observations shown Figure 3c.

Since surface steps on a Pt grain can have different orientations, nucleation at steps and growth along step edges can give rise to variations of the in-plane orientation between different graphene islands growing on the same Pt grain.[32,33] In the case of domains that are slightly rotated with respect to one another, the merging of growth fronts seems to preferentially lead to screw-dislocation induced growth of adlayers, while events in which only a single adlayer is formed, are relatively rare. A similar mechanism of dislocation-driven few layer growth has been reported for other two-dimensional materials.[34-37]

The fact that the 2nd and 3rd type of adlayer formation is not observed under quasi-equilibrium growth conditions is a consequence of the reduced local concentration of growth species. Indeed, the Pt catalyst in the local surrounding is already covered by the merging SLG domains. Only under non-equilibrium growth conditions, carbon growth species are sufficiently abundant to support growth of one or more adlayers by diffusion across the surface of the merged SLG domains.

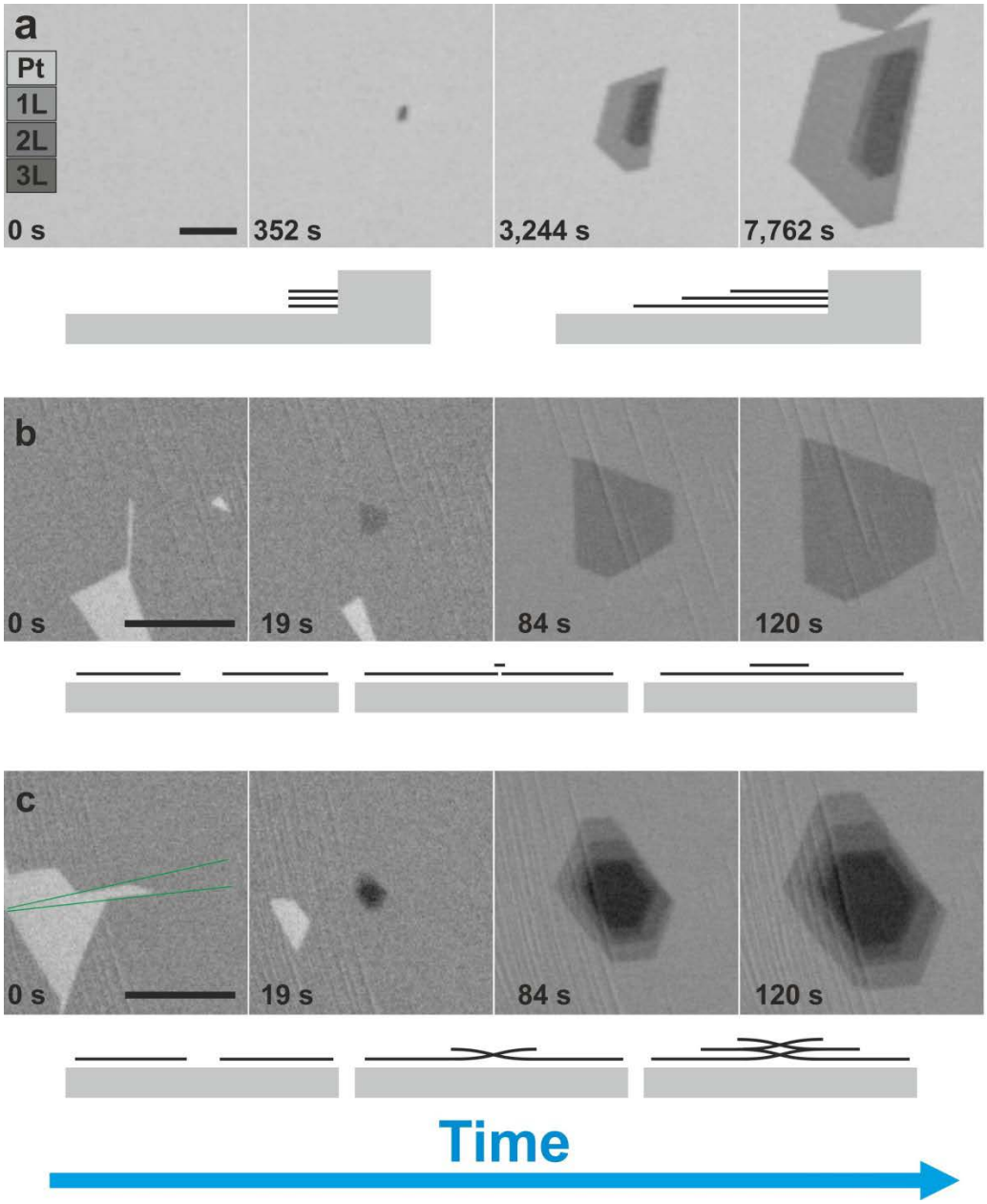

Figure 2. Mechanisms of adlayer formation: (a) *In situ* SEM images of FLG formed by adlayer nucleation at a Pt step. The schematic drawing highlights simultaneous nucleation and layer-dependent growth speed. **(b)** Nucleation of a single adlayer during the merging of two SLG islands with parallel growth fronts **(c)** Screw-dislocation induced formation of several adlayers. A schematic drawing of a cross-section through a screw dislocation based on TEM observations on GaN.[38] While adlayer formation according to (b) and (c) are only observed under non-equilibrium growth, simultaneous nucleation of several adlayers at a step is observed under both, quasi and non-equilibrium growth. The number of layers can be abstracted by comparing the contrast in the images with the contrast legend in (a). Scale bars, 2µm (a); 5µm (b, c).

3. Adlayer evolution

Direct observation of FLG growth reveals an interesting behavior that further helps understanding the underlying growth mechanism. Continuous imaging during experiments in which the temperature, pressure and gas feeding were kept constant, showed that the initial growth phase of FLG is followed by a phase during which the adlayers are shrinking (see Figure 4 and Supplementary Movie M5). Under both, quasi- and non-equilibrium growth conditions, the evolution of adlayers can thus be divided into a growth and an etching phase.

In the case of quasi-equilibrium growth, the transition from growth to etching is observed once the lateral distance between the adlayer growth front and the growth front of the first layer reaches around 2-5 µm (Figure 4a-c). The actual distance depends on the abundance of carbon growth species, their lifetime and associated diffusion length on the surface of the first layer, and is influenced by the local surface structure of the Pt grain. It is important to note that the reversal from growth to etching of the adlayer occurs while the first layer remains growing at unchanged rate (see figure 4 a-c). In the case of non-equilibrium growth, where the abundance of growth species is much higher, the switching from ALG growth to shrinking occurs only once most of the catalyst surface is coated by graphene (Figure 4d-f and Supplementary Movie M6).

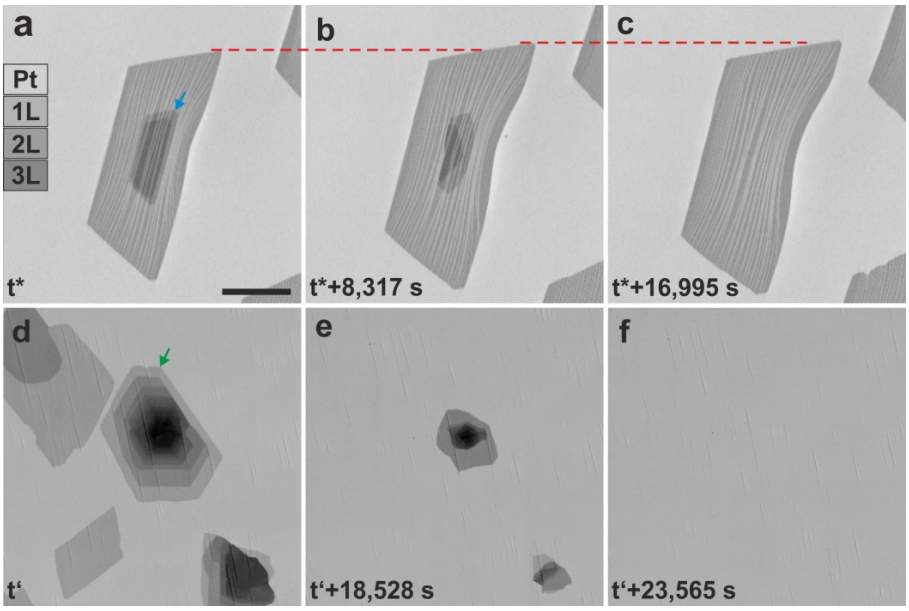

Figure 3. Shape evolution of adlayers during the shrinking phase: (a-c): Quasi-equilibrium growth: While the first layer continues expanding (see red dashed line), the adlayers (indicated by blue and green arrows) only grow up to a certain point and then start shrinking until they disappear. **(d-f)**: Non-equilibrium growth: Once most of the Pt surface is covered by SLG, the FLG domains start shrinking and disappear gradually. The number of layers can be abstracted by comparing the contrast in the images with the contrast legend. Scale bar in (a) measures 5µm.

Discussion:

In a previous work, we demonstrated that adlayers form on top of the initial layer the case of platinum.[23] The stacking sequence is thus such that the open edges of all layers are simultaneously exposed to the same environment. Growth reversal of an initially growing layer occurs when the forward reaction of carbon attachment at the growth front is overcome by the reverse reaction of carbon etching by the hydrogen. The plots in Figures 5a and 5b show the typical evolution of perimeter and area of a second-layer graphene island during extended exposure to quasi-equilibrium growth conditions. In the initial phase, adlayers grow in the attachment-limited regime and show a linear increase of the perimeter and a corresponding square-function like onset of the areal growth curve (Figure 4a). After the initial phase, the growth curve exhibits an inflection point and characteristics of a sigmoidal function (see also Figure 1e). The reason for the different growth behavior of the first and the adlayer sheets lies in their different initial growth speed. The first layer, which is in direct contact with the catalyst, has a lower energy due to the strong coupling with the Pt.[23] As a consequence, it grows substantially faster than the adlayers (see also Figure 1). Thus, the lateral distance between the adlayer growth front and the exposed active Pt catalyst increases with growth time. Accordingly, the number of growth species that reach the adlayer growth-front *via* diffusion across the surface of the first layer, decreases with time. This conclusion is underlined by the fact that the size difference between the adlayers decreases with adlayer number, pointing towards an exponential decay of growth species concentration with radial distance from the uncovered Pt substrate (see Fig. 1a, 3a). The diffusion and lifetime of growth species on the surface of graphene is thus the rate-limiting factor for the growth of adlayers, while the upwards hopping of growth species from layer to layer one does not seem to play a significant role. Since the competing hydrogen etching proceeds at relatively constant rate and is far less sensitive to the coverage of the catalyst, there is a point at which etching compensates the growth of adlayers. Further growth of the base layer causes the net etching speed of ALG to increase until it finally enters the detachment-limited regime that is characterized by constant reduction of the perimeter as shown by the green line in the inset of Figure 4b.

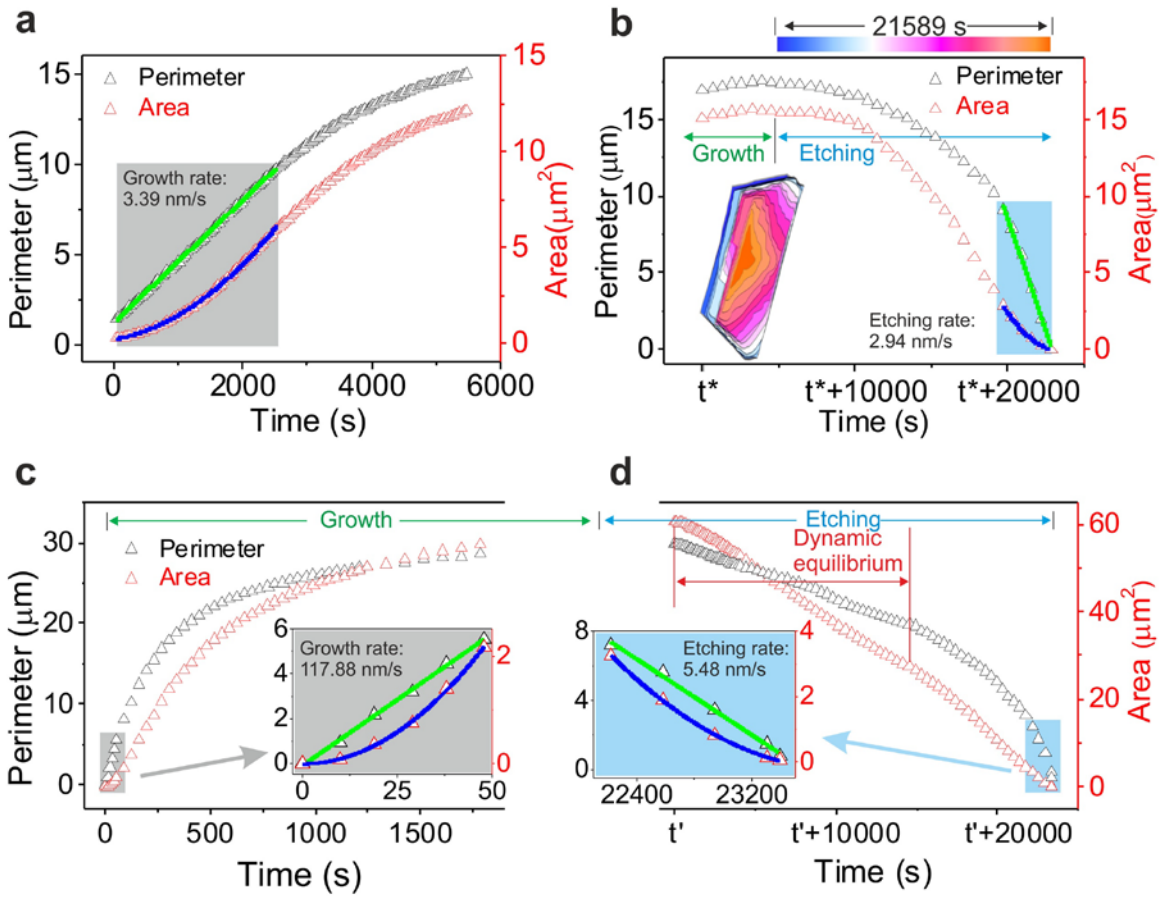

Figure 4: Evolution of ALG. (a,b): Diagrams showing the growth (a) and shrinking (b) phase of a second layer sheet under quasi-equilibrium growth. **(c, d)** show growth and etching under non-equilibrium growth. Insets in (c) and (d) show that initial growth is attachment limited and final etching is detachment limited, similar to the case of quasi-equilibrium growth.

The evolution of the perimeter and area of the second layer in the non-equilibrium growth regime is shown in Figures 4c and 4d. Although ALG formed by secondary nucleation in the non-equilibrium growth regime has a completely different structural origin, kinetically this ALG exhibits very similar behavior as ALG formed by direct nucleation. Again, the adlayers grow in the attachment limited regime during the initial growth phase (Figure 4c and inset in 4c). With increasing coverage of the catalyst, the rate of growth species production decreases. At the same time, the diffusion distance from the active catalyst to the adlayer growth fronts increases. Both together give rise to a slowing down of the growth speed and the observed sigmoidal growth behavior of the adlayers. Switching from growth to etching occurs once the rate of growth species attachment and hence, the forward direction of adlayer growth drops below the rate of carbon removal by hydrogen etching. The reversal from growth to etching occurs for the adlayer while the base layer is still growing. As can be seen in Figure 4d, the etching rate in terms of the areal change of the adlayer and thus, the number of carbon atoms gasified from the ALG per time, is roughly

constant at the beginning of the adlayer etching phase. Under continued feeding of C_2H_4 and H_2, a dynamic equilibrium will be established between the chemical potential of the gas phase and the one of the carbon species on the surface. The dynamic equilibrium is maintained until etching starts to be detachment limited. This happens when the integral sum of all adlayer perimeters, where etching takes place, falls below the value that is required to maintain the dynamic equilibrium. At this point, the etching rate at individual adlayers increases until etching gets detachment limited (the regime where the radius decreases linearly in Figure 4d).

In both, quasi- and non-equilibrium growth conditions, it is the drop of the forward reaction against a competing, fairly constant reverse reaction that ultimately leads to the disappearance of all adlayers. This is shown for the case of non-equilibrium growth conditions in Figure 5. Image 5a was recorded just before the polycrystalline Pt foil was completely covered by graphene. Image 5b shows an overview image containing the same region after complete etching of all adlayers after prolonged exposure to C_2H_4/H_2 feeding. It is very important to note that the delicate balance between growth and etching is layer dependent. While one of the advantages of direct industrial relevance is the possibility of producing purely single-layer graphene at full or partial coverage, we observed another important aspect. Indeed, the delicate balance between growth and etching has further implications. Close to full coverage, when growth species production is low, etching can attack weakly bound carbon atoms at grain boundaries and defects in the first layer. However, as soon as the catalyst is locally re-exposed, reactive growth species will be generated that tip the balance in favor of growth. This spontaneous back-and-forth cycling between etching of weakly bound carbon at defects and re-growth of stable graphene can be used for defect healing and the shifting of grain boundaries.[39,40]

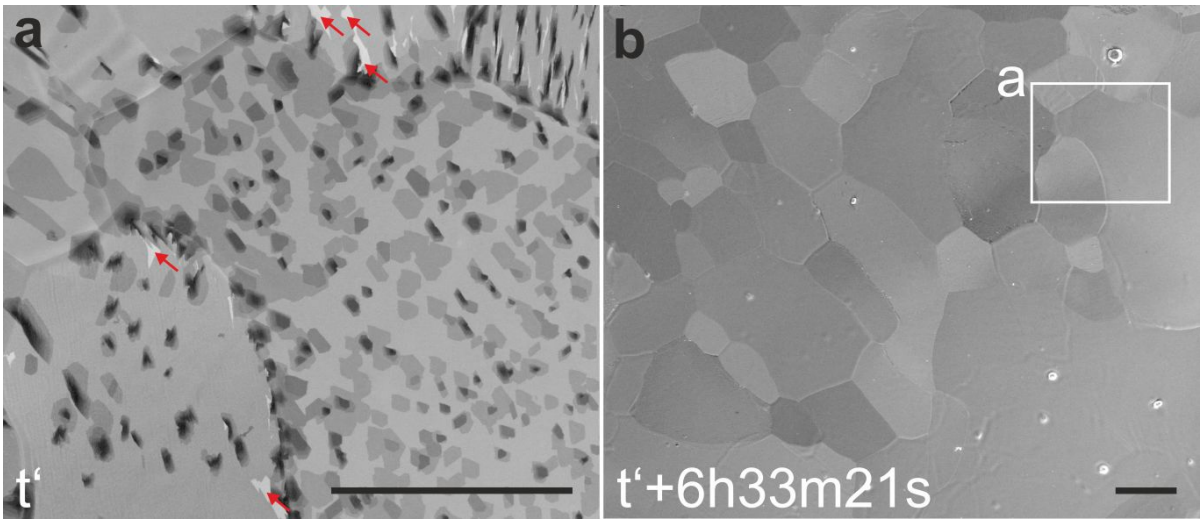

Figure 5. Complete removal of adlayers. **(a)** Graphene grown under non-equilibrium conditions on polycrystalline Pt foil showing FLG patches. The image was recorded moments before the Pt surface was

completely covered by graphene. The red arrows indicate bare Pt surface **(b)** Shows a large scale SLG covering the entire Pt surface after complete removal of adlayer graphene. The white square in (b) indicates the region where image (a) was recorded earlier. t' denotes the moment when Fig. 5a was recorded. CVD growth and image recording was performed under 1.2 sccm C_2H_4+10 sccm H_2 flow at 900 ˚C. The scale bars measure 100 µm.

In summary, we use real-time imaging during graphene CVD to observe a self-limited regime for single layer graphene growth on Pt foils. We reveal two fundamentally different types of graphene adlayer nucleation events. In addition to the standard primary nucleation process that occurs at the onset of growth, we report the first observation of secondary nucleation in graphene growth. Secondary nucleation is important because it is the result of dynamic interactions between already growing SLG domains, and because it occurs late, near full coverage, secondary nucleation events are likely to be the dominant factor leading to multilayer graphene growth on very clean surfaces. We show that the overall reaction outcome is determined by a dynamic equilibrium that sets up between the forward reaction step of graphene growth and the reverse reaction step of etching. If the dynamic equilibrium is tipped in favor of growth, the first layer that is in contact with the Pt surface grows faster than any of the adlayers. In contrast, adlayer growth gradually slows down, and while the bottom layer continuous to grow, the adlayers reverse direction and start etching and eventually, completely disappear. This growth reversal has an important practical consequence. It enables complete removal of adlayers and ensures that graphene growth is perfectly terminated at a single layer. The critical precondition for creating this dynamics for perfect single-layer graphene termination is a stronger coupling between the Pt surface and the first layer, than the interlayer coupling between the adlayers. This self-limiting growth can be easily realized on other metals that are characterized by similar or stronger graphene-surface coupling than Pt, such as Pd, Ru, Ir and Rh.[41-47] The dynamical features of this self-limiting growth mechanism are material independent, and can be implemented in any intrinsically layered growth that is typical for van der Waals type two-dimensional materials.

Acknowledgments

The contribution to this work by GE was supported by the U.S. Department of Energy, Office of Science, Basic Energy Sciences, Materials Sciences and Engineering Division.

References

(1) Hao, Y. F.; Bharathi, M. S.; Wang, L.; Liu, Y. Y.; Chen, H.; Nie, S.; Wang, X. H.; Chou, H.; Tan, C.; Fallahazad, B.; Ramanarayan, H.; Magnuson, C. W.; Tutuc, E.; Yakobson, B. I.; McCarty, K. F.; Zhang, Y. W.; Kim, P.; Hone, J.; Colombo, L.; Ruoff, R. S. *Science* **2013**, *342*, 720.
(2) Gao, L. B.; Ren, W. C.; Xu, H. L.; Jin, L.; Wang, Z. X.; Ma, T.; Ma, L. P.; Zhang, Z. Y.; Fu, Q.; Peng, L. M.; Bao, X. H.; Cheng, H. M. *Nat. Commun.* **2012**, *3*, 7.
(3) Chen, S. S.; Ji, H. X.; Chou, H.; Li, Q. Y.; Li, H. Y.; Suk, J. W.; Piner, R.; Liao, L.; Cai, W. W.; Ruoff, R. S. *Advanced Materials* **2013**, *25*, 2062.
(4) Sutter, P. W.; Flege, J. I.; Sutter, E. A. *Nat. Mater.* **2008**, *7*, 406.
(5) Pan, Y.; Zhang, H. G.; Shi, D. X.; Sun, J. T.; Du, S. X.; Liu, F.; Gao, H. J. *Advanced Materials* **2009**, *21*, 2777.
(6) Iwasaki, T.; Park, H. J.; Konuma, M.; Lee, D. S.; Smet, J. H.; Starke, U. *Nano Letters* **2011**, *11*, 79.
(7) Au, C. T.; Ng, C. F.; Liao, M. S. *J. Catal.* **1999**, *185*, 12.
(8) Lang, B. *Surf. Sci.* **1975**, *53*, 317.
(9) Sutter, P.; Sadowski, J. T.; Sutter, E. *Phys. Rev. B* **2009**, *80*, 10.
(10) Nie, S.; Walter, A. L.; Bartelt, N. C.; Starodub, E.; Bostwick, A.; Rotenberg, E.; McCarty, K. F. *Acs Nano* **2011**, *5*, 2298.
(11) Nie, S.; Wofford, J. M.; Bartelt, N. C.; Dubon, O. D.; McCarty, K. F. *Phys. Rev. B* **2011**, *84*, 7.
(12) Sutter, P.; Ciobanu, C. V.; Sutter, E. *Small* **2012**, *8*, 2250.
(13) Sutter, P.; Hybertsen, M. S.; Sadowski, J. T.; Sutter, E. *Nano Letters* **2009**, *9*, 2654.
(14) Sutter, P.; Sutter, E. *Adv. Funct. Mater.* **2013**, *23*, 2617.
(15) Wofford, J. M.; Nie, S.; McCarty, K. F.; Bartelt, N. C.; Dubon, O. D. *Nano Letters* **2010**, *10*, 4890.
(16) Mu, R.; Fu, Q.; Jin, L.; Yu, L.; Fang, G.; Tan, D.; Bao, X. *Angewandte Chemie-International Edition* **2012**, *51*, 4856.
(17) Yao, Y.; Fu, Q.; Zhang, Y. Y.; Weng, X.; Li, H.; Chen, M.; Jin, L.; Dong, A.; Mu, R.; Jiang, P.; Liu, L.; Bluhm, H.; Liu, Z.; Zhang, S. B.; Bao, X. *Proc. Natl. Acad. Sci. U. S. A.* **2014**, *111*, 17023.
(18) Addou, R.; Dahal, A.; Sutter, P.; Batzill, M. *Appl. Phys. Lett.* **2012**, *100*.
(19) Cui, Y.; Fu, Q.; Zhang, H.; Tan, D. L.; Bao, X. H. *J. Phys. Chem. C* **2009**, *113*, 20365.
(20) Dong, G. C.; Frenken, J. W. M. *Acs Nano* **2013**, *7*, 7028.
(21) Patera, L. L.; Africh, C.; Weatherup, R. S.; Blume, R.; Bhardwaj, S.; Castellarin-Cudia, C.; Knop-Gericke, A.; Schloegl, R.; Comelli, G.; Hofmann, S.; Cepek, C. *Acs Nano* **2013**, *7*, 7901.
(22) Peng, Z.; Somodi, F.; Helveg, S.; Kisielowski, C.; Specht, P.; Bell, A. T. *J. Catal.* **2012**, *286*, 22.
(23) Wang, Z. J.; Dong, J. C.; Cui, Y.; Eres, G.; Timpe, O.; Fu, Q.; Ding, F.; Schloegl, R.; Willinger, M. G. *Nat. Commun.* **2016**, *7*.
(24) Wang, Z.-J.; Weinberg, G.; Zhang, Q.; Lunkenbein, T.; Klein-Hoffmann, A.; Kurnatowska, M.; Plodinec, M.; Li, Q.; Chi, L.; Schloegl, R.; Willinger, M.-G. *ACS nano* **2015**, *9*, 1506.
(25) Kidambi, P. R.; Bayer, B. C.; Blume, R.; Wang, Z.-J.; Baehtz, C.; Weatherup, R. S.; Willinger, M.-G.; Schloegl, R.; Hofmann, S. *Nano Letters* **2013**, *13*, 4769.
(26) Blume, R.; Kidambi, P. R.; Bayer, B. C.; Weatherup, R. S.; Wang, Z.-J.; Weinberg, G.; Willinger, M.-G.; Greiner, M.; Hofmann, S.; Knop-Gericke, A.; Schloegl, R. *Physical Chemistry Chemical Physics* **2014**, *16*, 25989.
(27) Ma, T.; Ren, W.; Liu, Z.; Huang, L.; Ma, L.-P.; Ma, X.; Zhang, Z.; Peng, L.-M.; Cheng, H.-M. *Acs Nano* **2014**, *8*, 12806.
(28) Weatherup, R. S.; Shahan, A. J.; Wang, Z. J.; Mingard, K.; Pollard, A. J.; Willinger, M. G.; Schloegl, R.; Voorhees, P. W.; Hofmann, S. *Nano Letters* **2016**, *16*, 6196.
(29) Meca, E.; Lowengrub, J.; Kim, H.; Mattevi, C.; Shenoy, V. B. *Nano Letters* **2013**, *13*, 5692.

(30) Shu, H. B.; Tao, X. M.; Ding, F. *Nanoscale* **2015**, *7*, 1627.
(31) Zhang, X.; Li, H.; Ding, F. *Advanced Materials* **2014**, *26*, 5488.
(32) Loginova, E.; Nie, S.; Thuermer, K.; Bartelt, N. C.; McCarty, K. F. *Phys. Rev. B* **2009**, *80*.
(33) Starodub, E.; Bostwick, A.; Moreschini, L.; Nie, S.; El Gabaly, F.; McCarty, K. F.; Rotenberg, E. *Phys. Rev. B* **2011**, *83*, 9.
(34) Morin, S. A.; Forticaux, A.; Bierman, M. J.; Jin, S. *Nano Letters* **2011**, *11*, 4449.
(35) Xia, J.; Zhu, D. D.; Wang, L.; Huang, B.; Huang, X.; Meng, X. M. *Adv. Funct. Mater.* **2015**, *25*, 4255.
(36) Thurmer, K.; Bartelt, N. C. *Phys. Rev. B* **2008**, *77*.
(37) Wang, F.; Wang, X. D. *Nanoscale* **2014**, *6*, 6398.
(38) Yang, H.; Lozano, J. G.; Pennycook, T. J.; Jones, L.; Hirsch, P. B.; Nellist, P. D. *Nat. Commun.* **2015**, *6*.
(39) Rogge, P. C.; Thuermer, K.; Foster, M. E.; McCarty, K. F.; Dubon, O. D.; Bartelt, N. C. *Nat. Commun.* **2015**, *6*.
(40) Tyurnina, A. V.; Okuno, H.; Pochet, P.; Dijon, J. *Carbon* **2016**, *102*, 499.
(41) Preobrajenski, A. B.; Ng, M. L.; Vinogradov, A. S.; Martensson, N. *Phys. Rev. B* **2008**, *78*, 4.
(42) Siller, R. H.; Oates, W. A.; McLellan, R. B. *Journal of the Less-Common Metals* **1968**, *16*, 71.
(43) Arnoult, W. J.; McLellan, R. B. *Scripta Metallurgica* **1972**, *6*, 1013.
(44) Yuan, Q. H.; Gao, J. F.; Shu, H. B.; Zhao, J. J.; Chen, X. S.; Ding, F. *J. Am. Chem. Soc.* **2012**, *134*, 2970.
(45) Kim, H. W.; Ku, J.; Ko, W.; Jeon, I.; Kwon, H.; Ryu, S.; Kahng, S. J.; Lee, S. H.; Hwang, S. W.; Suh, H. *Carbon* **2014**, *78*, 190.
(46) Wei, D. S.; Wang, F. *Surf. Sci.* **2012**, *606*, 485.
(47) Lacovig, P.; Pozzo, M.; Alfe, D.; Vilmercati, P.; Baraldi, A.; Lizzit, S. *Physical Review Letters* **2009**, *103*, 4.